IIETA International Information and Engineering Technology Association
Advancing the World of Information and Engineering

Traitement du Signal
Vol. 42, No. 1, February, 2025, pp. 291-302
Journal homepage: http://iieta.org/journals/ts

Developed Improved Weighed Quantum Particle Swarm Optimisation with Deep Convolutional Neural Network Algorithm to Improve the Automated Concrete Surface Defect Detection in Bridge Inspections

Vinodhini Veerasamy[1*], Suresh Kumar Paramasivam[2], Kavitha Ramaswami Jothi[1]

[1] Department of Electronics and Communication Engineering, University College of Engineering, Ariyalur 607106, India
[2] Department of Civil Engineering, University College of Engineering, Panruti 607106, India

Corresponding Author Email: vinsjeyam@gmail.com

https://doi.org/10.18280/ts.420125

Received: 19 June 2024
Revised: 20 November 2024
Accepted: 14 January 2025
Available online: 28 February 2025

Keywords:
concrete surface defect detection, automated bridge inspection, Deep Convolutional Neural Network (DCNN), IWQPSO, feature selection, hyperparameter optimization, Gazebo robot simulators

ABSTRACT

Natural calamities like storms and earthquakes can pose a threat to bridges. The main technique for finding imperfections in bridges is observing them with unequipped eyes. This approach is laborious, risky, and exposes testers to the dangers of falling. Consequently, digital bridge inspections are required. Reports of inspection for bridges typically concentrate on fractures. Many building materials with fractured surfaces are situated at high elevations or over fluid, making them difficult for a bridge inspector to reach. Lack of illumination beneath bridges and a complicated visual backdrop might make it more difficult for testers to see and quantify cracks. A novel approach Improved Weighed Quantum Particle Swarm Optimisation (IWQPSO) with Deep Convolutional Neural Network (DCNN) method with Gazebo robot simulators proposed to enhance automated concrete surface defect detection in bridge inspections. It makes use of border trading, and stochastic change, including predictable initialization. This study proposes an approach for Unmanned Aerial Vehicle (UAV) photogrammetry-based bridge inspections regarding communication channels. This allows for secure and uninterrupted access to the higher levels of the buildings without causing traffic problems. Information is acquired using a unique image acquisition procedure that has been systematized and standardized.

1. INTRODUCTION

UAVs are aircraft that function without an actual human operator present. To convey private information during the procedure of aerial surveillance and structural surveillance, UAV networks are built and deployed [1]. A novel dynamic planning of paths and an obstacle-avoiding technique for UAVs have been presented. UAVs are also a practical option for business and civil uses. UAVs can be utilized for in-storm weather tests, obstacle rescue operations, real-time hazard surveillance, and vital infrastructure surveillance [2]. In situations where manned helicopters are at present utilized, such as field surveillance, getting a bird's-eye view of a significant exercise or information incident, determining the progression of forests, tracking speeds chase, pursuing fleeing lawbreakers, or keeping an eye on the progress of city demonstrations, UAVs might be able to provide a low-cost alternative [3]. Many of these uses for tiny UAVs necessitate that they be able to negotiate in difficult terrain, where routing or installation might include a high number of obstacles of various sizes or orientations. The context of rescue and search operations is one instance when remote vehicle operation could be acceptable [4]. Few research has examined panoramic image merging for bridge inspection, even though many have concentrated on creating computational image processing and algorithms for machine learning for autonomous hazard diagnosis [5]. Regular monitoring and inspections of these kinds of buildings are necessary both before and following development [6]. A variety of stakeholders, including the shareholders, managers of projects, designers, engineers, builders, suppliers, consumers, and managers of facilities, frequently inspect the construction to monitor and evaluate it. Personality and a large degree of heterogeneity in evaluation quality are further characteristics of inspection by hand [7]. Certain circumstances could be dangerous for people, like a bridge's decking, something that is vulnerable to a storm or earthquake, or an examination at an elevated level. The needs and difficulties faced by various inspection and surveillance tasks vary [8]. Cracks can be found manually by observing and evaluating shown in Figure 1. Infrastructure inspectors use conventional detection techniques to assess the degree of degradation based on their expertise. The procedure is time-consuming, laborious, along risky. It is necessary to create automatic and impartial procedures to circumvent the limitations of the current standard approach [9]. UAVs can effortlessly fly near connected elements that would be challenging for humans to reach. By using the included camera on the UAV, bridge cracks may be detected through UAV footage. The recording device can be operated remotely from the ground's perspective [10]. Finding concrete surface defects during bridge examinations is essential to preserving the structural

soundness and security of the structures supporting bridges [11].

Infrastructure maintenance, particularly bridge inspections, is critical for ensuring public safety and infrastructure longevity. Concrete structures, the backbone of many bridges, are prone to surface defects such as cracks, spalling, scaling, and delamination due to environmental exposure, load stress, and aging. Bridge inspections are conducted manually by skilled inspectors, but these methods are time-intensive, subjective, and prone to human error. Manual inspections can pose safety risks, especially in hard-to-reach areas, and are often unable to comprehensively cover large bridge structures within limited timeframes. Automated defect detection using computer vision and machine learning (ML) has emerged as a promising alternative, offering scalability, speed, and consistent results. Among these, DCNNs are particularly effective due to their ability to learn hierarchical features from raw image data, achieving state-of-the-art performance in many image-based classification and localization tasks.

The motivation for this work stems from the pressing need to enhance the accuracy, efficiency, and reliability of detecting concrete surface defects in bridge inspections. Traditional manual methods are labour-intensive, prone to human error, and often inconsistent, particularly in large-scale or complex infrastructures. Automated systems leveraging deep learning models, such as DCNNs have shown promise in defect detection but face challenges like sensitivity to hyperparameters, difficulty handling environmental noise, and scalability issues [12, 13].

The main contributions of this work are:

Development of the IWQPSO algorithm for efficient hyperparameter tuning, leveraging quantum-inspired weighted mechanisms for faster and more accurate optimization.

Design and implementation of a DCNN model tailored for defect detection in concrete surfaces, incorporating advanced feature extraction techniques and regularization strategies.

Integration of the IWQPSO-DCNN hybrid framework to address challenges like defect variability, environmental noise, and scalability.

Extensive evaluation of real-world datasets, demonstrating superior accuracy, efficiency, and robustness compared to baseline methods.

2. PROPOSED SYSTEM

The novel method IWQPSO-DCNN proposed to prevent inaccurate information and/or data loss. A systematized and standardized recommended image capture technique is used for information collecting in this research. Integrating Gazebo with UAVs opens up a wide range of possibilities for simulating and testing UAV-related algorithms and applications [14-16]. Both simulators provide realistic environments where UAVs can be virtually deployed, allowing researchers and developers to experiment with various scenarios without the cost and risk associated with real-world testing. In these simulations, users can model different types of UAVs, such as quadcopters, fixed-wing aircraft, or even hybrid designs, along with their sensors, actuators, and control systems. Simulate tasks like navigation, path planning, obstacle avoidance, surveillance, and payload delivery in diverse environments. Gazebo being open-source and highly customizable is widely used in the robotics community for simulating UAVs. It offers a rich set of features, including physics engines for realistic flight dynamics, sensor simulation (e.g., cameras, LiDAR, GPS), and integration with Robot Operating System (ROS) for seamless development and testing of UAV control algorithms. It also supports UAV simulation and offers a user-friendly graphical interface for building complex robotic systems. It provides a variety of pre-built models and environments, making it easier to get started with UAV simulations [16].

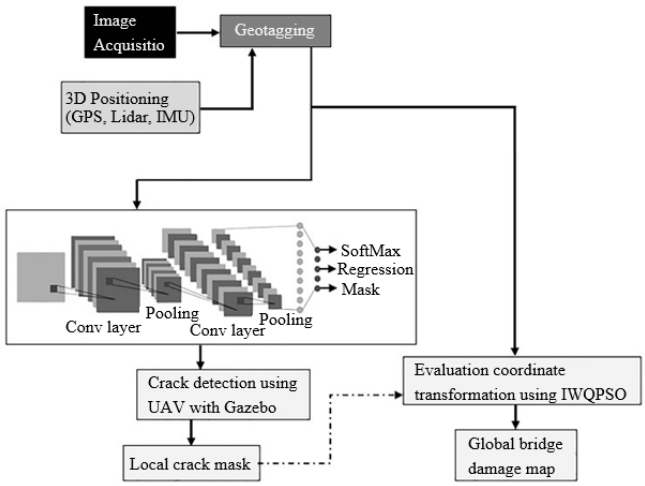

Figure 1. The overall scheme of the proposed method

Figure 1 depicts the general layout of the proposed strategy, which is broken down into three phases. A quick and inexpensive Image Capturing and Geo-Tagging (ICGT) that can effectively handle intermediary operations was created to gather referencing information from photos concurrently [17, 18]. The proposed system is for rapidly identifying cracks and harm recognition in the subsequent phase of crack-damaged recognition for offline inspection images. Every image's DCNN outcomes are obtained using its geotagged place. To create a Global Bridge Damage Map (GBDM), the images are immediately projected onto a global location. Machines have been implemented for five distinct purposes in the context of infrastructure and buildings project inspection and observation: (a) preservation inspection; (b) quality control during construction examination; (c) Model built; (d) progress observation; and (e) security examination.

2.1 Dataset collection

Similar to photogrammetry, visual imaging focuses on the collection of images, videos, and other types of visual data. Typically, still image cameras, video cameras, smartphones, and other devices are used to obtain these. A sample of the information gathered and information gathered utilizing a UAV equipped with visual imagery technology is shown in Figure 2. Data collection within Gazebo involves capturing sensor readings, images, and telemetry data generated by the virtual UAVs during their missions. Annotations may also be added to the data to indicate target objects, waypoints, or other relevant information. Gazebo provides a powerful platform for generating high-fidelity UAV datasets that can facilitate the development and evaluation of robust machine-learning algorithms for UAV applications. An investigation showed that aerial images obtained from Gazebo through the UAV system for pavement fracture inspection were more reliable

than those gathered from more conventional sources, such as static photos and crack depth measurement instruments [19-20]. The research used a five-stage inspection process that included damage proof of identity, drone-enabled bridge evaluation, data inspection, and location risk evaluation.

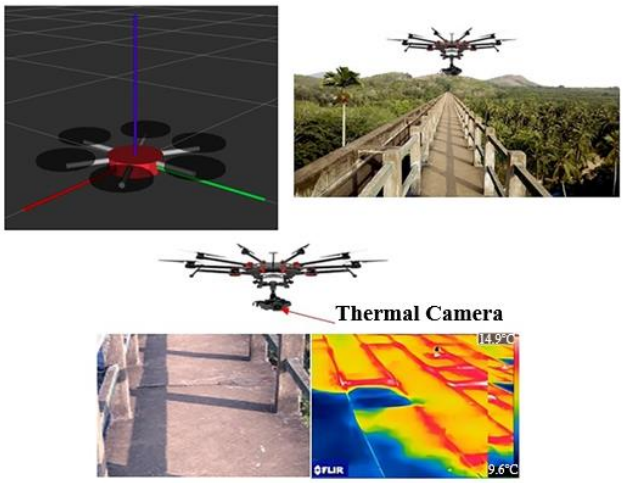

Figure 2. Equipment IR-UAV with Gazebo and its sample thermal data

2.2 Infrared thermal imaging

Equipment Gazebo with IR-UAV and its sample thermal data collected are shown in Figure 3. Due to the disruption of heat transfer caused by delamination areas above it will be determined to be hotter than similar areas above soundness concrete [19]. An infrared camera placed on a low-altitude airplane was used to capture thermal images of two concrete bridge decks. The underlying defect locations detected by the Gazebo with the IRT-UAV system have been verified by conventional methods including hammering sound and Half-Cell Potential (HCP).

Figure 3. Gazebo with UAV equipment model

Table 1 provides the dataset format and information necessary for the development, testing, and validation of the creation and inspection of the DIWQPSO-DCNN method. The essential elements required for creating and evaluating the DIWQPSO-DCNN algorithm are included in the data table structure. Table 2 shows the sample data and its description for developing the algorithm, every column comprises an image sample together with its distinctive characteristics, raw image information, defect kind, defect location, seriousness straight, metadata, beforehand processed information, recovered vectors of characteristics, and real-world labeling [21].

Table 1. Dataset description

Component	Description
Image ID	Unique identifier for each image in the dataset.
Image data	High-resolution images of concrete surfaces captured using drones or cameras
Defect type	Label indicating the type of defect (e.g., crack, spalling, scaling).
Defect location	Coordinates or region in the image where the defect is located
Defect severity	Classification of defect severity (e.g., minor, moderate, severe).
Metadata	Additional information about the images (e.g., date, time, location of capture).
Pre-processed data	Images after preprocessing steps such as normalization, resizing, and augmentation
Feature vectors	Extracted features from images used for training the DCNN.
Ground truth labels	Manually annotated labels used for training and validation
Training set	Subset of the dataset used for training the DCNN, including image data and corresponding labels.
Validation set	The subset of the dataset used for tuning hyperparameters and validating model performance
Test set	Subset of the dataset used for evaluating the final model's performance
Hyperparameters	Parameters optimized using DIWQPSO for the DCNN (e.g., learning rate, number of layers, batch size).
Performance metrics	Metrics used to evaluate the model's performance (e.g., accuracy, precision, recall, F1-score).
Optimization results	Results of the DIWQPSO algorithm, including optimal hyperparameters and feature selection outcomes.

Table 2. Sample datasets

Image ID	Image Data	Defect Type	Defect Location	Defect Severity	Metadata	Pre-processed Data	Feature Vectors	Ground Truth Labels
IMG_001	(image data binary)	Crack	(120, 80, 150, 100)	Moderate	{date: "2024-01-01", location: "Bridge A"}	(preprocessed data)	[0.5, 0.3, 0.8, ...]	Crack
IMG_002	(image data binary)	Spalling	(60, 30, 110, 90)	Severe	{date: "2024-01-02", location: "Bridge B"}	(preprocessed data)	[0.7, 0.4, 0.9, ...]	Spalling
IMG_003	(image data binary)	Scaling	(100, 50, 130, 70)	Minor	{date: "2024-01-03", location: "Bridge C"}	(preprocessed data)	[0.6, 0.2, 0.7, ...]	Scaling
IMG_004	(image	Crack	(140, 90,	Severe	{date: "2024-01-04",	(preprocessed	[0.8, 0.5,	Crack

	data binary)		180, 120)		location: "Bridge D"}	data)	0.4, ...]	
IMG_005	(image data binary)	Spalling	(50, 20, 80, 60)	Moderate	{date: "2024-01-05", location: "Bridge E"}	(preprocessed data)	[0.3, 0.6, 0.8, ...]	Spalling
IMG_006	(image data binary)	Scaling	(70, 40, 90, 70)	Severe	{date: "2024-01-06", location: "Bridge F"}	(preprocessed data)	[0.5, 0.7, 0.3, ...]	Scaling
IMG_007	(image data binary)	Crack	(110, 70, 150, 110)	Minor	{date: "2024-01-07", location: "Bridge G"}	(preprocessed data)	[0.4, 0.6, 0.9, ...]	Crack
IMG_008	(image data binary)	Spalling	(80, 50, 120, 80)	Severe	{date: "2024-01-08", location: "Bridge H"}	(preprocessed data)	[0.7, 0.8, 0.6, ...]	Spalling
IMG_009	(image data binary)	Scaling	(100, 60, 130, 90)	Moderate	{date: "2024-01-09", location: "Bridge I"}	(preprocessed data)	[0.5, 0.3, 0.4, ...]	Scaling
IMG_010	(image data binary)	Crack	(130, 80, 170, 120)	Severe	{date: "2024-01-10", location: "Bridge J"}	(preprocessed data)	[0.6, 0.9, 0.7, ...]	Crack
IMG_011	(image data binary)	Spalling	(40, 10, 70, 50)	Minor	{date: "2024-01-11", location: "Bridge K"}	(preprocessed data)	[0.3, 0.5, 0.7, ...]	Spalling
IMG_012	(image data binary)	Scaling	(90, 30, 120, 70)	Severe	{date: "2024-01-12", location: "Bridge L"}	(preprocessed data)	[0.8, 0.4, 0.9, ...]	Scaling
IMG_013	(image data binary)	Crack	(120, 90, 160, 130)	Moderate	{date: "2024-01-13", location: "Bridge M"}	(preprocessed data)	[0.6, 0.5, 0.3, ...]	Crack
IMG_014	(image data binary)	Spalling	(60, 40, 90, 70)	Severe	{date: "2024-01-14", location: "Bridge N"}	(preprocessed data)	[0.7, 0.3, 0.6, ...]	Spalling
IMG_015	(image data binary)	Scaling	(80, 20, 100, 50)	Moderate	{date: "2024-01-15", location: "Bridge O"}	(preprocessed data)	[0.4, 0.8, 0.5, ...]	Scaling

2.3 Data acquisition

An instance of a sensor-embedded Gazebo with UAV and the information it collects is shown in Figure 3. The deflection of beams was examined using a Gazebo with a UAV system equipped with a reflecting prism, whose location was monitored by a laser-tracking complete station [22]. The ceiling effect aerodynamic examination, developed using the use of Computational Fluid Dynamics (CFD) was used to optimize the Gazebo with UAV architecture. The Gazebo with UAV made use of the effect of the ceiling to its advantage to make connections and carry out its surveillance tasks of data acquisition is shown in Figure 4.

Several processes, comprising image extraction, preliminary processing, extracting features, and labeling, are involved in the information collection method used in the development of the IWQPSO-DCNN [21, 22].

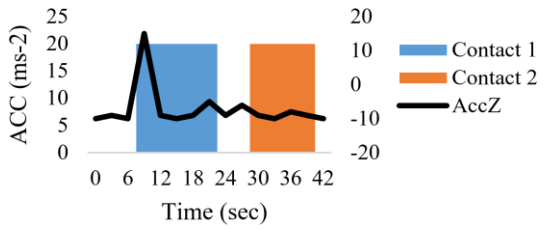

Figure 4. Sensor embedded in Gazebo with UAV for data acquisition based on contact

2.3.1 Image capture

High-resolution images of concrete surfaces are captured using drones or stationary cameras equipped with high-resolution and thermal imaging capabilities [23-26]. The following equation describes the resolution of the captured image:

$$\text{Resolution} = \frac{\text{No. of Pixels}}{\text{Image Area}} \tag{1}$$

2.3.2 Image pre-processing

Pre-processing steps are applied to the raw images to enhance quality. Normalization, resizing, and augmentation were done for pre-processing the data.

Normalization:

$$X_{norm}(i,j) = \frac{X(i,j) - \min(X)}{\max(X) - \min(X)} \tag{2}$$

where, $X(i,j)$ is pixel (x, y) intensity value; min(X) and max(X) are minimum and maximum intensity values in the image.

Resizing:

The images are resized to a standard size suitable for the DCNN, for example, 256 × 256 pixels.

Augmentation:

By applying techniques such as random rotations, flips, scaling, and noise addition to the concrete surface images, we can generate a more extensive and varied dataset from the limited available images. This augmentation helps in simulating various real-world conditions and defects, making the model more robust and capable of identifying defects under different scenarios and lighting conditions [23].

2.4 Feature extraction

Feature extraction is a crucial step in the process of building and optimizing machine learning models, particularly in fields such as image processing, natural language processing, and signal processing.

Convolution Operation:

$$F_{xy} = \sum_{m=1}^{M} \sum_{n=1}^{N} X_{(x+m-1)(y+n-1)} \cdot K_{mn} \quad (3)$$

where, X is the input image, K is the convolution kernel (filter) of size $M \times N$, and F is the output feature map.

Activation Function (ReLU):

$$f(x) = \max(0, x) \quad (4)$$

Max Pooling Operation:

$$P_{xy} = max_{m,n} F_{(x+m)(y+n)} \quad (5)$$

where, P is the pooled feature map.

Labelling: Manual labelling of the images involves identifying and categorizing defects such as cracks, spalling, and scaling. Each defect is annotated with its location and severity [27, 28].

Bounding Box Annotation:

$$(i_1, j_1, i_2, j_2) \quad (6)$$

where, (i_1, j_1) and (i_2, j_2) are coordinates of the bounding box around the defect.

2.5 Dataset structuring

The labelled data is structured into a dataset suitable for training and testing the IWQPSO-DCNN.

Splitting of dataset

Training Set Size = 0.7 × Total Dataset Size

Validation Set Size = 0.2 × Total Dataset Size

Test Set Size = 0.1 × Total Dataset Size

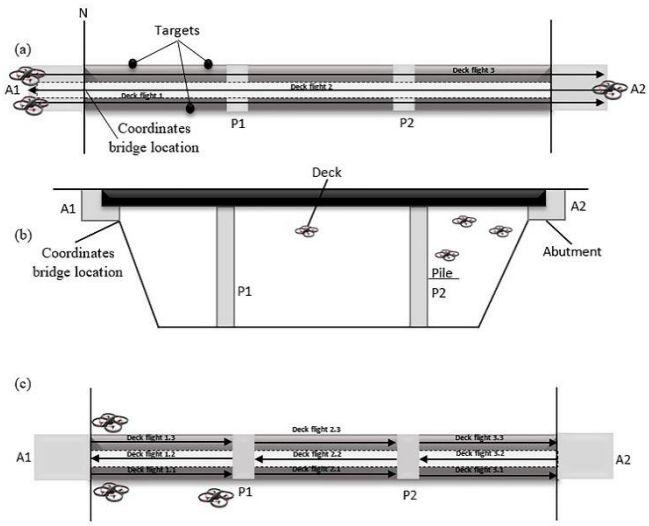

Figure 5. (a) Acquisition of image; (b) Abutments (A1 and A2) and piers (P1 and P2); and (c) deck and bridge location

Based on the discoveries made by the drones during the examination flights, some suggestions are offered for the systematization of collecting information for routine visual examinations. Certain Gazebo with UAVs might not be able to navigate some areas of a bridge, including the area between pillars or the elastomeric bearings pad. The bridge's laterals, the highest point, and bottom sections ought to be examined. Take images of a bridge check, starting with the first abutment and going through all of the intermediary columns. The bridge placement and flight sequencing will be ascertained by its measurements shown in Figure 5.

2.6 Proposed system

The measurement of the crack width in images was based on these two techniques. The information used to train the crack recognition model included open-source fracture information, camera-equipped Gazebo in UAVs, and smartphones shown in Figure 6. To ascertain the precision of the proposed model and confirm the viability of the proposed approach, the depths of the derived outlines were determined and contrasted with the real values shown in Figure 7.

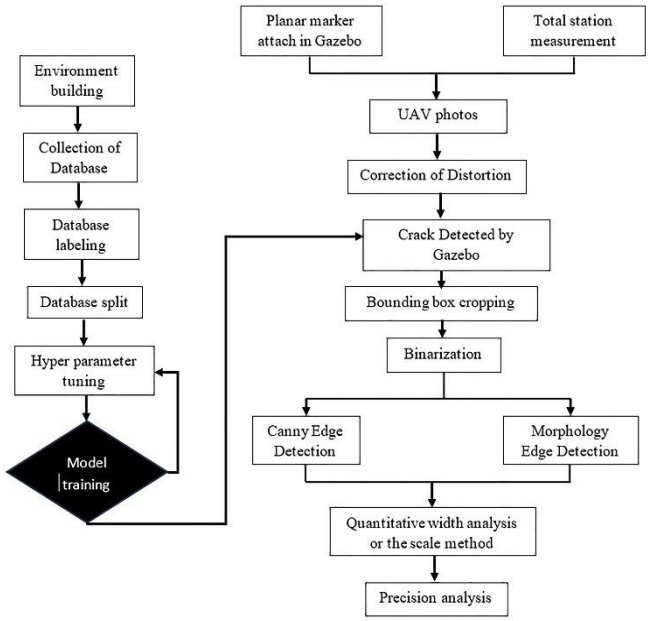

Figure 6. The process of Gazebo with UAV took photos of bridge

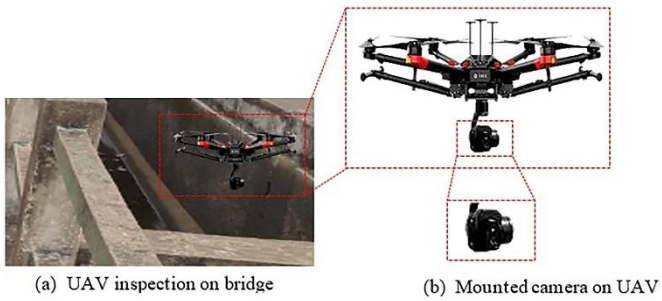

(a) UAV inspection on bridge (b) Mounted camera on UAV

Figure 7. Operation of Gazebo with UAV bridge inspection

Figure 8 displays the ICGT's software foundation. During the inspection, the ICGT can be started or stopped remotely from a station using the command line utility service is part of the ROS core tool chain. It should be noted that these two jobs

operate concurrently at 5 frames per second to synchronize the information from the sensors and the photos [29, 30]. The process keeps running cyclically until the central controller issues the instruction to "Stop".

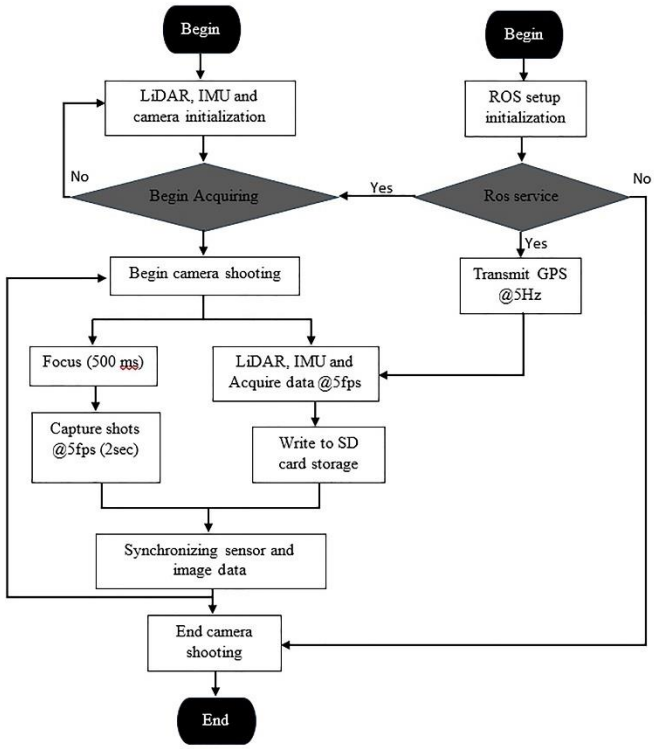

Figure 8. Process of ICGT software on bridge inspection

2.6.1 Feature points of measurement and planar marker

The fracture widths in the photos were measured using the scale method. Planar markings are difficult to install on reinforced concrete structures since the majority of them are raised motorways or span rivers. The features of the concrete surfaces were measured using a total location, and the resulting positions were utilized as a substitute for planar markings in the opposite calculation of the spatial distances shown in Figure 9.

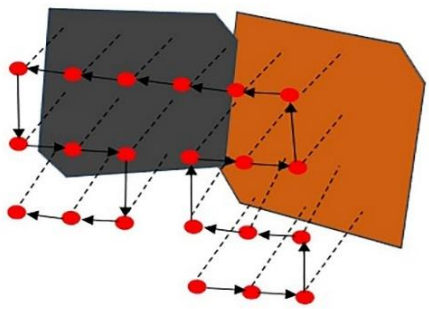

Figure 9. Initialization of particle using back-and-forth path

Every particle is first given a random positioning and speed. It then moves by updating both the swarm's best position (G_k) and its best previous position (P_k). Let i_k and v_k represent a particle's location and velocity at generation k, accordingly. In the following generations, that particle's velocity and location are determined by:

$$v_{k+1} \leftarrow w.v_k + \varphi_1.r_1.(P_k - i_k) + \varphi_2.r_2.(G_k - i_k) \quad (7)$$

$$i_{k+1} \leftarrow i_k + v_{k+1} \quad (8)$$

where, r_1 and r_2 are selected at random of an identical distribution in the interval [0, 1], w is the inertial coefficient, φ_1 is the cognitive coefficient, and v_k is the social coefficient. According to Eqs. (7) and (8), the movement of a particle involves a trade-off between traveling in the direction of its best prior position, going in the direction of its path, or going in the direction of the swarm's optimal position. The coefficients of w, φ_1, and φ_2 establish the ratio among selections.

Algorithm: IWQPSO-DCNN

A hybrid model of IWQPSO-DCNN was proposed to enhance the computerized identification of surface concrete faults in bridge inspections. Using the optimized IWQPSO-DCNN model, the procedure includes feature selection, hyperparameter optimization, and fault identification.

Step 1. Initialization

{

1.1. Particle Initialization: Initialize a swarm of N particles, where each particle represents a potential solution with a set of hyperparameters and selected features for the DCNN. Randomly initialize the position X and velocity V_x of each particle.

$$I_x = (i_{x1}, i_{x2}, \dots, i_{xD}) \quad (9)$$

$$V_x = (v_{x1}, v_{x2}, \dots, v_{xD}) \quad (10)$$

where, x = 1, 2, ..., N and D - dimensionality of a number of hyperparameters and features.

1.2. Quantum Initialization: Initialize the quantum position Q_x for each particle.

$$Q_x = \frac{1}{\sqrt{2\pi\sigma^2}} e^{\sigma - \frac{(i_x - \mu)^2}{2\pi^2}} \quad (11)$$

}

Step 2. Fitness Evaluation

{

2.1. Training the DCNN: Train the DCNN model with the hyperparameters and features represented by each particle. Use the training dataset to perform forward and backward propagation.

2.2. Fitness Function: The fitness function f can be defined as the negative of the validation loss or a performance metric like accuracy or F1-score.

$$f(I_x) = \text{Validation Loss } (\text{DCNN}(I_x)) \quad (12)$$

}

Step 3: Update Particle Positions and Velocities

{

3.1. Velocity Update: Update the velocity of each particle using the quantum-inspired velocity equation.

$$V_x^{t+1} = w.V_x^t + c_1.r_1.(P_x - I_x^t) + c_2.r_2.(P_x - I_x^t) + c_3.r_3.(Q_x - I_x^t) \quad (13)$$

where, w is inertia weight; $c_1, c_2, and\ c_3$ are coefficients of acceleration; $r_1, r_2, and\ r_3$ are random numbers between 0 and 1; P_x is local best position; G is global best position.

3.2. Position Update:
Update the position of each particle.

$$I_x^{t+1} = I_x^t + V_x^{t+1} \quad (14)$$

}
Step 4: Quantum Position Update
{
Quantum Update: Update the quantum position of each particle based on the new position.

$$Q_x^{t+1} = \frac{1}{\sqrt{2\pi\sigma^2}} e^{\sigma - \frac{(i_x^{t+1} - \mu)^2}{2\pi^2}} \quad (15)$$

}
Step 5. Iterative Optimization
{
5.1. Convergence Check: Repeat steps 2 to 4 until convergence criteria are met
5.2. Select Optimal Hyperparameters and Features: The global best position G represents the optimal hyperparameters and feature set for the DCNN.
}
Step 6. Final Model Training and Evaluation
{
6.1. Train and evaluate Final DCNN: Train the DCNN with the optimal hyperparameters and selected features on the entire training dataset.
}
The IWQPSO-DCNN method can increase the precision and dependability of automatic concrete surface detection of imperfections for bridge examinations by implementing this method to optimize the hyperparameters and feature choice process.

2.7 Crack identification using IWQPSO-DCNN model training

A one-stage approach uses packed forecasting, while a two-stage model uses sparse forecasting. Compared to a one-stage model, the prediction results of a two-stage model are sparser because a select search is used to choose an established amount of areas of interest shown in Figure 10.

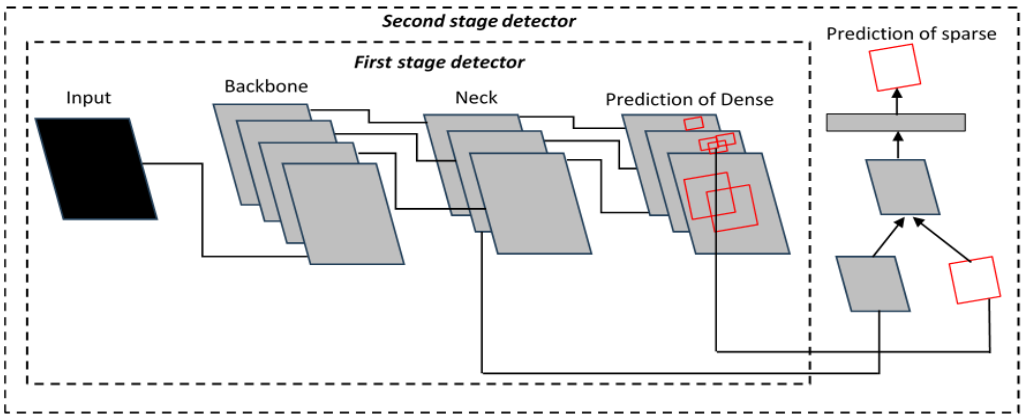

Figure 10. Multi-stage model detector

The fracture is represented by the black line in the centre of the image, and the bounding boxes for object detection are represented by the black frames [31-33]. The bounding box that gave image measurements based on the notion that the image's top-left corner is its point of origin is shown in Figure 11. One might extract the bounding box range and carry out image enhancement shown in Figure 12.

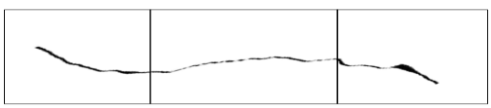

Figure 11. Crack detected by crack

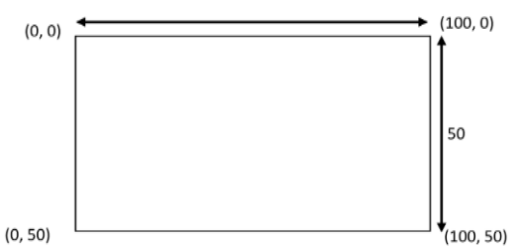

Figure 12. Bounding box output

2.8 Inspections form

Other kinds are chosen based on the substance of every single bridge element such as the abutment, section, deck, wires, parapet/handrail, or pavement must be used to express the inspection findings regarding every one of these elements. The following categories of substances have been established in this study to streamline the process for as long as possible: (M) masonry, (REW) reinforced earth walls, (C) concrete, (S) metal, and (CB) cables.

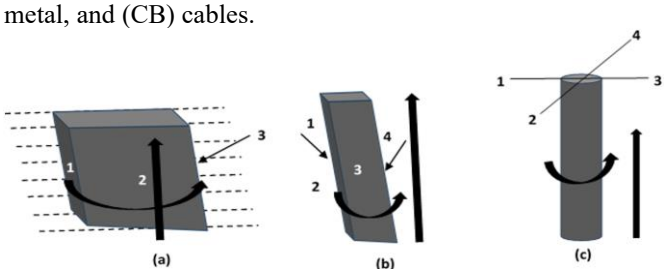

Figure 13. Image acquisition of Gazebo in UAV (a) first abutment (b) pier or column in parallel (c) pier or column in cylindrical manner

Figure 13 shows the column inspection done from the bottom up and in an anticlockwise direction on every side. To

achieve this, a list of the most frequent damages has been established, ones that could impact all varieties of building materials and components and of which the Gazebo UAV operator needs to be aware when conducting the inspection.

3. RESULTS AND DISCUSSIONS

Management and autonomous technologies should be developed in future studies. Gazebo Robots are also successful agents because of their dependability and acceleration, which guarantees that the information that stakeholders have access to is current and reliable. This information can assist robots in autonomously determining the navigational objectives that satisfy human needs.

3.1 Indoor test

The first inspection is conducted in an indoor setting and restricted to evaluating the LiDAR system when the motorized aircraft is stable. The chamber measures 4, 7, and 3 meters in width, width, and size, correspondingly. The spaces that separate the room's dropping tiles of the ceiling are apparent as seen in Figure 14(a)-(e). These gaps have a width of roughly 2 cm is more than the estimated inaccuracy.

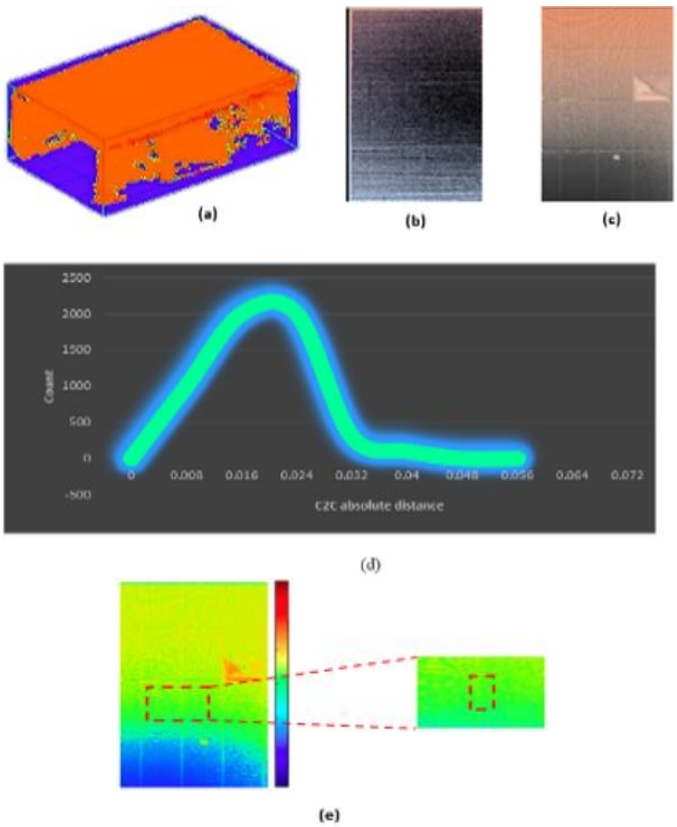

Figure 14. Test results at the initial stage (a) Design the platform to generate a point on cloud (b) Point cloud segment (c) Segment reference (d) Histogram distance comparison and (e) Comparison of a colored segment from segment reference based on distance

3.2 Outdoor inspection

The bridge deck was the site of the outside examination. Investigators looked for crack deterioration on the foundations, the exterior, and the bottom beneath the bridge. Figure 15 depicts the overall view of the bridge that is undergoing inspections by the Gazebo robot. Figure 16 displays the recognition outcomes of the IWQPSO-DCNN approach, indicating that the mAP attained 92%.

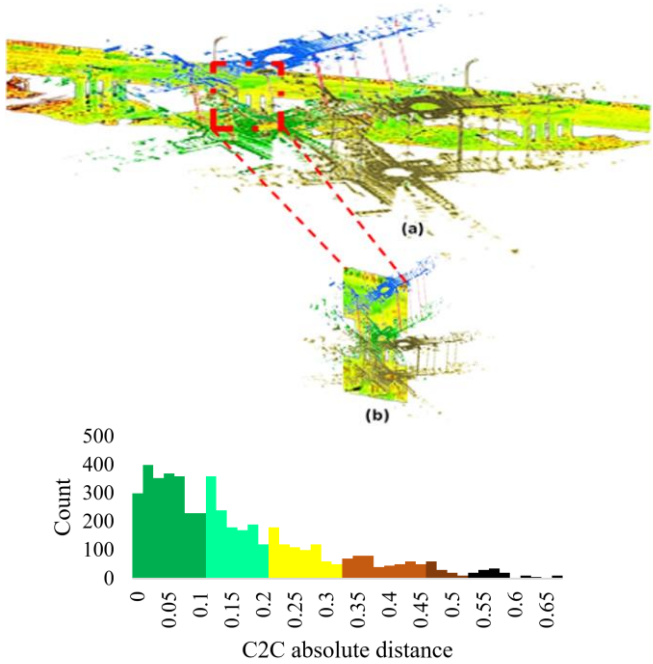

Figure 15. Both of the clouds of points individually synchronized with one another

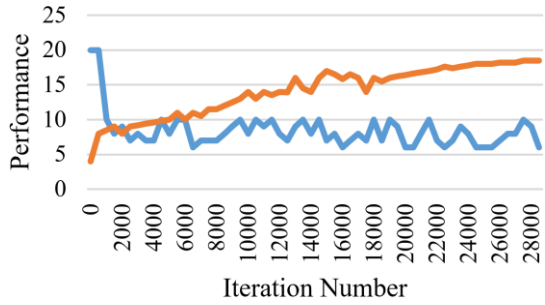

Figure 16. Model training results by Gazebo robot

3.3 Identification of crack images

The crack detection findings are displayed in Figure 17, and the image recognition findings may be categorized into images with varying lighting and background noise.

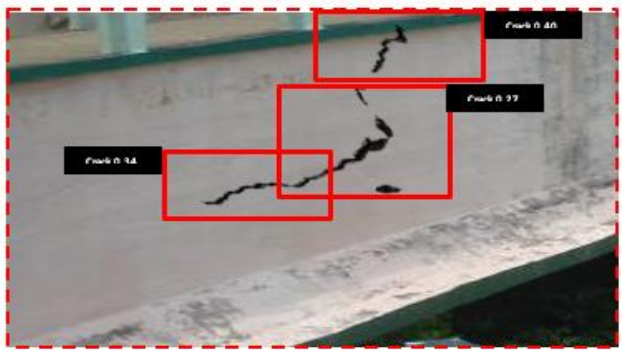

Figure 17. Crack identification outcome by Gazebo robot

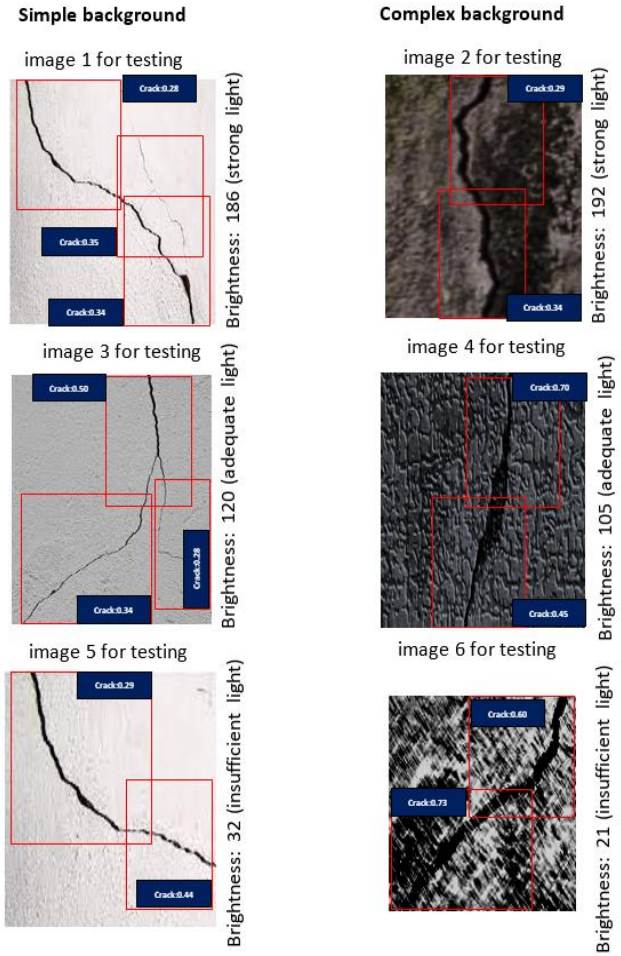

Figure 18. Crack recognition outcomes

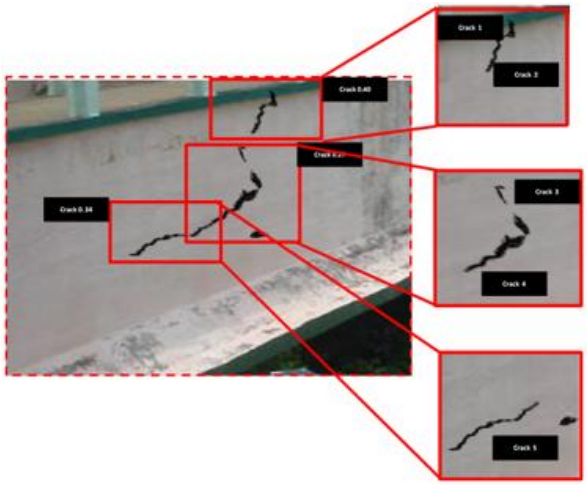

Figure 19. Bounding box cropping by Gazebo robot

The IWQPSO-DCNN approach's crack recognition outcomes, as shown in Figure 18 unequivocally show that the proposed algorithm is capable of identifying cracks in images using Gazebo robot. Since there were often three separate images per crack in every image when the image annotations records were prepared 3 bounding boxes might have been produced. A snapshot of the boundary frame characteristics and locations indicated by Gazebo robot in Figures 19 and 20. The percentage that represents the trust that the observed feature is a crack enclosed in boxes.

Damage M6 is associated with the mineral precipitation in joints exhibited a moderate degree of degeneration and a minimal amount of extending (some locations approximately 10–50%). This led to the assignment of risk A2/B2, demonstrating that the corrective criteria suggestion relates to new, regular checks, the duration of which will depend on the bridge's age. Damage C4 or rust stains resulting from a lack of protection in architectural encouragement was found on the deck and showed signs of mild damage progressing with only 10% to 50% of the damaged area. Given that the width of the rust linear spots was greater than 5 mm, the destruction grade was high to extremely high. Two tripod markers were positioned as fixed markers in the center of the bridge before the drone's flight. Drone flights used these markers as their points of reference. The environment was gloomy in the morning and bright in the afternoon throughout the examination time.

These different light levels could cause problems for the bridge's 3D architecture. The crack dataset is created by labeling crack locations on reduced images shown in Figure 20. To enable automated per-pixel separation of fractures, efficient network topologies have been created with the geometries of crack separation in consideration shown in Figure 20 and Table 3. When in binary format and serialized, records are effective for loading large data sets and facilitating simple transmission and accessibility [32]. Records make it possible to store sequence information in a manner that makes it straightforward and effective to import, such as phrase-encoded information or sequences of time shown in Figure 21. In comparison to CNN, DCNN, and RNN, the proposed IWQPSO-DCNN method maintains the best accuracy, sensitivity, specificity, and Precision shown in Table 4. In comparison to existing models, the IWQPSO-DCNN method greatly enhances the automated identification of concrete imperfections in the surface during bridge inspections, yielding greater precision and dependable findings [29-30].

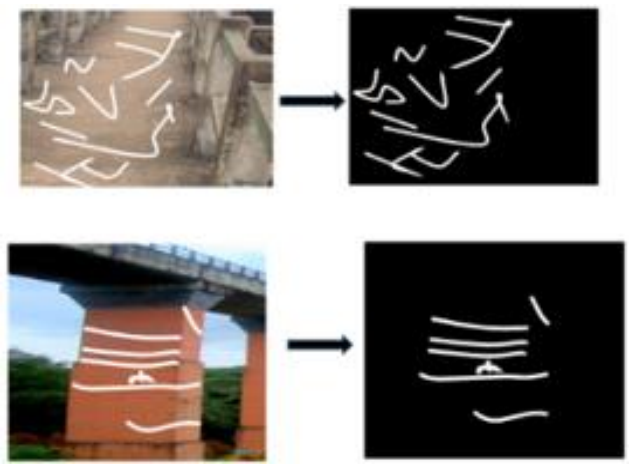

Figure 20. Gazebo Robot view in UAV (a) Top view of bridge drone image (b) Top view of labeled image (c) supporting drone image of the bridge (d) supporting bridge labeled image

Table 3. Cracks

Crack	27	Crack	33	Crack	40
Left X	11	Left X	293	Left X	558
Top Y	118	Top Y	58	Top Y	93
Width	337	Width	252	Width	369
Height	133	Height	369	Height	129

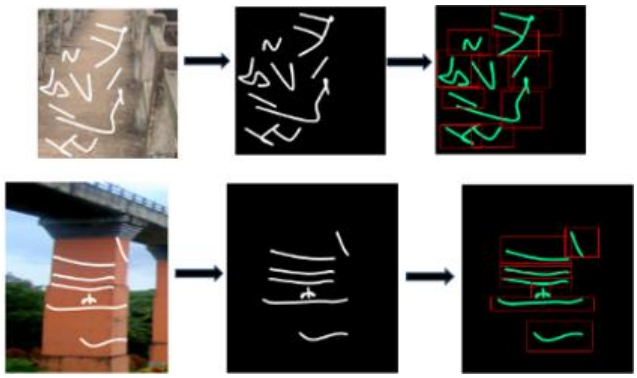

Figure 21. Gazebo robot operations on (a) Bridge supporting drone image (b) Contours trace (c) Bounding box extraction (d) Bridge deck drone image (e) Contours trace drone image (f) Bounding box bridge extraction

Table 4. Performance measures

Model	Accuracy	Sensitivity (Recall)	Specificity	Precision
CNN	86.3	83.6	88.0	81.5
DCNN	90.1	87.2	92.3	85.0
RNN	84.5	82.1	86.6	79.9
Proposed IWQPSO-DCNN	94.2	92.5	95.7	90.8

3.4 Performance measures

In comparison to CNN, DCNN, and RNN, the proposed IWQPSO-DCNN system has the greatest F1 score demonstrating a solid balance between remembering and precision and, consequently, improved overall effectiveness in identifying defects shown in Table 5. The proposed IWQPSO-DCNN system learns the recurring patterns and characteristics that correspond to cement imperfections in the surface with the maximum precision during training (94.2%), demonstrating its excellent performance on the training dataset [24,, 25]. The training and validation accuracy is shown in Table 6.

Table 5. Performance measures of F1-score, AUC and MSE

Model	F1-Socre	AUC	MSE
CNN	82.5	0.88	0.033
DCNN	86.7	0.92	0.026
RNN	80.5	0.87	0.036
Proposed IWQPSO-DCNN	91.3	0.96	0.020

Table 6. Performance measures of training and validation accuracy

Model	Training Accuracy	Validation Accuracy
CNN	88.0	86.3
DCNN	92.0	90.5
RNN	86.0	84.6
Proposed IWQPSO-DCNN	95.3	94.2

Outperforming CNN, DCNN, and RNN, the proposed IWQPSO-DCNN system gets the smallest loss during learning (0.120), demonstrating that it successfully minimizes the number of errors on its training database. The computerized identification of cement surface flaws during bridge inspections is greatly improved by including the IWQPSO-DCNN method offers lower training and validation loss than conventional neural network models shown in Table 7.

Table 7. Performance measures of training and validation loss

Model	Training Loss	Validation Loss
CNN	0.231	0.271
DCNN	0.181	0.211
RNN	0.251	0.291
Proposed IWQPSO-DCNN	0.121	0.151

4. CONCLUSIONS

The proposed pipeline can potentially be expanded to identify failures in structures such as overhead electrical lines and railroads. It may additionally adapt and harness the benefits of Gazebo Robot in UAVs. The integration of a UAV equipped with a Gazebo Robot simulation and utilizing an IWQPSO-DCNN significantly enhances automated concrete surface defect detection in bridge inspections. This approach improves defect detection accuracy, as the combination of IWQPSO- DCNN allows for precise tuning of neural network parameters, effectively identifying defects such as cracks and spalling. IWQPSO offers efficient optimization, improving convergence rates and reducing the likelihood of being trapped in local minima, common in traditional optimization techniques. The Gazebo Robot simulation environment enables the testing and validation of the UAV's navigation and inspection capabilities in a realistic yet controlled setting, ensuring the system can perform real-time defect detection effectively. This combination results in a robust, accurate, and efficient solution for bridge inspection and maintenance [33-35].

REFERENCES

[1] Chen, C., Cao, L., Chen, Y., Chen, B., Yue, Y. (2024). A comprehensive survey of convergence analysis of beetle antennae search algorithm and its applications. Artificial Intelligence Review, 57(6): 141. https://doi.org/10.1007/s10462-024-10789-0

[2] Wu, T., Cheng, X., Yan, Z., Yang, J., Chai, X., Dai, X. (2024). Acoustic tunnel lining cavity detection using cepstral coefficients with optimized filter bank. Measurement Science and Technology, 35(6): 066115. https://doi.org/10.1088/1361-6501/ad30be

[3] Yang, S., Zhou, L., Wang, C., Wang, S., Lv, J., Wang, Q. (2023). Research on SF-YOLONet metal gear end-face defect detection method based on evolutionary algorithm optimization. Research Square. https://doi.org/10.21203/rs.3.rs-3420533/v1

[4] Chen, H., Zhang, Z., Yin, W., Zhou, G., et al. (2024). Shape characterization and depth recognition of metal cracks based on laser infrared thermography and machine learning. Expert Systems with Applications, 238: 122083. https://doi.org/10.1016/j.eswa.2023.122083

[5] Hassani, S., Dackermann, U. (2023). A systematic review of optimization algorithms for structural health monitoring and optimal sensor placement. Sensors,

23(6): 3293. https://doi.org/10.3390/s23063293
[6] Xu, Y., Xiong, B., Ma, W., Liu, Y. (2023). Software-defined nanophotonic devices and systems empowered by machine learning. Progress in Quantum Electronics, 89: 100469. https://doi.org/10.1016/j.pquantelec.2023.100469
[7] Chaupal, P., Rajendran, P. (2023). A review on recent developments in vibration-based damage identification methods for laminated composite structures: 2010-2022. Composite Structures, 311: 116809. https://doi.org/10.1016/j.compstruct.2023.116809
[8] Keshmiry, A., Hassani, S., Mousavi, M., Dackermann, U. (2023). Effects of environmental and operational conditions on structural health monitoring and non-destructive testing: A systematic review. Buildings, 13(4): 918. https://doi.org/10.3390/buildings13040918
[9] Afshar, A., Nouri, G., Ghazvineh, S., Hosseini Lavassani, S.H. (2024). Machine-learning applications in structural response prediction: A review. Practice Periodical on Structural Design and Construction, 29(3): 03124002. https://doi.org/10.1061/PPSCFX.SCENG-1292
[10] Imran, M.M.H., Jamaludin, S., Ayob, A.F.M., Ali, A.A.I.M., et al. (2023). Application of artificial intelligence in marine corrosion prediction and detection. Journal of Marine Science and Engineering, 11(2): 256. https://doi.org/10.3390/jmse11020256
[11] Ivanova, S., Kuznetsov, A., Zverev, R., Rada, A. (2023). Artificial intelligence methods for the construction and management of buildings. Sensors, 23(21): 8740. https://doi.org/10.3390/s23218740
[12] Qiu, Y., Zhang, Z. (2023). Civil engineering structural damage identification by integrating benchmark numerical model and pcnn network. IEEE Access, 11: 130815-130827. https://doi.org/10.1109/ACCESS.2023.3334628
[13] Kapoor, N.R., Kumar, A., Kumar, A., Kumar, A., Arora, H.C. (2024). Artificial intelligence in civil engineering: An immersive view. In Artificial Intelligence Applications for Sustainable Construction, pp. 1-74. https://doi.org/10.1016/B978-0-443-13191-2.00009-2
[14] Imran, M.M.H., Ali, A.A.I.M., Jamaludin, S., Mohamad, A.F. (2023). The application of artificial intellegence in corrosion monitoring. Journal of Engineering and Science Research, 7(1): 17-25. https://doi.org/10.26666/rmp.jesr.2023.1.4
[15] Angelis, D., Sofos, F., Karakasidis, T.E. (2023). Artificial intelligence in physical sciences: Symbolic regression trends and perspectives. Archives of Computational Methods in Engineering, 30(6): 3845-3865. https://doi.org/10.1007/s11831-023-09922-z
[16] Prasad, M.A., Subiramaniyam, N.P. (2023). Multilevel thresholding for multi-spectral image using convolutional fuzzy clustering algorithm and gradient multilayer kernelized perceptron. International Journal of Intelligent Systems and Applications in Engineering, 11(7s): 580-592.
[17] Tao, J., Li, Z., Chen, C., Liang, R., Wu, S., Lin, F., Cheng, Z.J., Yan, B.B., Chen, G.Y. (2024). Intelligent technologies powering clean incineration of municipal solid waste: A system review. Science of the Total Environment, 935: 173082. https://doi.org/10.1016/j.scitotenv.2024.173082
[18] Akewar, M., Chandak, M. (2023). Hyperspectral imaging algorithms and applications: A review. TechRxiv, 1-35. https://doi.org/10.36227/techrxiv.24743562.v2
[19] Jia, H., Yang, F., Li, T., Suresh Kumar, R. (2023). Target recognition and detection system based on sensor and nonlinear machine vision fusion. Nonlinear Engineering, 12(1): 20220310. https://doi.org/10.1515/nleng-2022-0310
[20] Makhadmeh, S.N., Al-Betar, M.A., Doush, I.A., Awadallah, M.A., Kassaymeh, S., Mirjalili, S., Zitar, R.A. (2023). Recent advances in Grey Wolf Optimizer, its versions and applications. IEEE Access, 12: 22991-23028. https://doi.org/10.1109/ACCESS.2023.3304889
[21] Ma, S., Du, Y., Wang, S., Su, Y. (2023). Application of machine learning in material corrosion research. Corrosion Reviews, 41(4): 417-426. https://doi.org/10.1515/corrrev-2022-0089
[22] Chen, G., Shi, W., Yu, L., Huang, J., Wei, J., Wang, J. (2024). Wireless sensor placement optimization for bridge health monitoring: A critical review. Buildings, 14(3): 856. https://doi.org/10.3390/buildings14030856
[23] Learning, U.D., Swain, B.K., Chowdhary, C.L., Gain, R. (2023). Indian Sign Language. Investigations in Pattern Recognition and Computer Vision for Industry 4.0. IGI Global Publisher of Timely Knowledge.
[24] Hidayat, M.I.P., Pramata, A.D., Airlangga, P.P. (2023). Finite element and generalized regression neural network modelling of multiple cracks growth under the influence of multiple crack parameters. Multidiscipline Modeling in Materials and Structures, 19(5): 1014-1041. https://doi.org/10.1108/MMMS-03-2023-0105
[25] Raval, M.S., Roy, M., Kaya, T., Kapdi, R. (Eds.). (2023). Explainable AI in Healthcare: Unboxing Machine Learning for Biomedicine. CRC Press.
[26] Abas, H.A., Nasir, N. (2024). Drone patrolling applications, challenges, and its future: A review. SSRN. https://doi.org/10.2139/ssrn.4682937
[27] Iavich, M., Kuchukhidze, T., Gagnidze, A. (2024). Novel post-quantum digital signature using verkle trees and lattices. Scientific and Practical Cyber Security Journal, 8(1): 1-13.
[28] Ponnusamy, S., Assaf, M., Antari, J., Singh, S., Kalyanaraman, S. (2024). Digital Twin Technology and AI Implementations in Future-Focused Businesses. IGI Global.
[29] El Makhloufi, A. (2023). AI application in transport and logistics: Opportunities and challenges (an exploratory study). CoE City Net Zero, Faculty of Technology, Amsterdam Univeristy of Applied Sciences.
[30] Zhao, N., Wei, J., Long, Z., Yang, C., Bi, J., Wan, Z., Dong, S. (2023). An integrated method for tunnel health monitoring data analysis and early warning: Savitzky–Golay smoothing and wavelet transform denoising processing. Sensors, 23(17): 7460. https://doi.org/10.3390/s23177460
[31] Hossain, K.A. (2023). Analysis of present and future use ofartificial intelligence (AI) in line of fouth industrial revolution (4IR). Scientific Research Journal, 11(8): 1-50.
[32] Wu, P., Yang, L., Li, W., Huang, J., Xu, Y. (2023). Construction safety risk assessment and early warning of nearshore tunnel based on BIM technology. Journal of Marine Science and Engineering, 11(10): 1996. https://doi.org/10.3390/jmse11101996

[33] Steininger, M. (2023). Deep learning for geospatial environmental regression. Doctoral Dissertation, Universität Würzburg. https://opus.bibliothek.uni-wuerzburg.de/frontdoor/index/index/docId/31312.
[34] Bull, L.A., Abdallah, I., Mylonas, C., Avendaño-Valencia, L.D., et al. (2023). Data-centric monitoring of wind farms: Combining sources of information. In Data Driven Methods for Civil Structural Health Monitoring and Resilience, pp. 120-180.
[35] Assmann, R., Caldwell, D., Cerullo, G., Chapman, H., et al. (2024). Physics for health. In EPS Grand Challenges: Physics for Society in the Horizon 2050. https://doi.org/10.1088/978-0-7503-6342-6ch5

NOMENCLATURE

IWQPSO	Improved Weighed Quantum Particle Swarm Optimisation
DCNN	Deep Convolutional Neural Network
UAV	Unmanned Aerial Vehicle
ROS	Robot Operating System
ICGT	Image Capturing and Geo-Tagging
GBDM	Global Bridge Damage Map
HCP	Half-Cell Potential
CFD	Computational Fluid Dynamics